IEEE Access
Multidisciplinary | Rapid Review | Open Access Journal

Received 7 July 2024, accepted 14 July 2024, date of publication 16 July 2024, date of current version 25 July 2024.

Digital Object Identifier 10.1109/ACCESS.2024.3429418

RESEARCH ARTICLE

MPPT-SAZE Algorithm for Solar PV Array Powered Series-Connected 5-Phase Induction Motors Supplied Off a Z-Source and Dual-Inverter

SAAD KHADAR[1], ALMOATAZ Y. ABDELAZIZ[2], (Senior Member, IEEE), Z. M. S. ELBARBARY[3], AND MAHMOUD A. MOSSA[4]

[1]Laboratory of Applied Automation and Industrial Diagnosis, Ziane Achour University of Djelfa, Djelfa 17000, Algeria
[2]Faculty of Engineering and Technology, Future University in Egypt, Cairo 11835, Egypt
[3]Department of Electrical Engineering, College of Engineering, King Khalid University, Abha, Saudi Arabia
[4]Electrical Engineering Department, Faculty of Engineering, Minia University, Minia 61111, Egypt

Corresponding authors: Saad Khadar (saad.khadar@univ-djelfa.dz) and Mahmoud A. Mossa (mahmoud_a_mossa@mu.edu.eg)

This work was supported by the Deanship of Scientific Research, King Khalid University, through the General Research Project, under Grant RGP.2/33/45.

ABSTRACT This paper proposes a new single-stage solution for solar photovoltaic (PV) array powered series-connected 5-phase induction motors (SC5PIM) under open-end winding (OEW) supplied off a Z-source and dual-inverter, where the Z-source converter serves dual purposes. The first purpose is of maximum power point tracking (MPPT) by adjusting the duty ratio based on a sample-averaged zero-sequence elimination (SAZE) method in order to extract optimum power from the PV modules. Whereas the second purpose it serves is to feed the dual-inverter system of the SC5PIM-OEW topology, which has been investigated for the first time. Furthermore, the dual-Inverter system of SC5PIM-OEW topology is controlled using space vector pulse width modulation (SVPWM) technique with rotor flux-oriented control (FOC) strategy in order to produce a very high reliable adjustable speed drive system. The proposed topology and designed controller were modeled to run on the FPGA in real-time, using the OPAL-RT 4500 simulator under different environmental conditions. Simulation results clearly show that the designed controller can effectively track the rotor speed and obtain good dynamic performance, where the maximum and average error values are less than 0.5 rad/s of the reference speed signal during various conditions.

INDEX TERMS MPPT technique, open-end winding, SAZE scheme, series-connected 5-phase induction motors, solar PV array, Z-source converter, dual-inverter system.

NOMENCLATURE

Acronyms:

PV	Solar Photovoltaic.
SC5PIM	Series-Connected 5-Phase Induction Motors.
OEW	Open-End Winding.
MPPT	Maximum Power Point Tracking.
SAZE	Sample-Averaged Zero-Sequence Elimination.
FOC	Flux Oriented Control.
SVPWM	Space Vector Pulse Width Modulation.
VSI	Voltage Source Inverter.
ZSC	Z-Source Converter.

Symbols:

$V_{aa'} V_{bb'} V_{cc'} V_{dd'}, V_{ee'}$	The stator voltages (V).
$i_{aa'}, i_{bb'}, i_{cc'} i_{dd'} i_{ee'}$	The stator currents (A).
R_{s1}, R_{s2}	The stator resistances (Ω).
R_{r1}, R_{r2}	The rotor resistances (Ω).
L_{s1}, L_{s2}	The stator inductances (H).
L_{r1}, L_{r2}	The rotor inductances (H).
$M_1 M_2$	The mutual inductances (H).
T_{em1}, T_{em2}	The electromagnetic torque (Nm).

The associate editor coordinating the review of this manuscript and approving it for publication was Reinaldo Tonkoski.

V_{pv} The PV cell voltage (V).
I_{pv} The generated PV current (A).
S_M The switching function.
D The shoot through duty ratio.
H The boost factor.
V_z The output voltage of Z-source (V).
m_a The modulation index.

I. INTRODUCTION

Today, much research is focused on using renewable sources, like solar photovoltaic (PV), wind, fuel cells, thermo-generators, and others, to supply the unending and growing demand for electrical energy [1], [2]. The sun is one of the cleanest and most renewable energy sources accessible; when it is used, it generates neither harmful waste nor greenhouse gasses. Therefore, using photovoltaic technology to provide the necessary electricity can be a good substitute, especially for water pumps, electric fans, and air compressors [3], [4].

Numerous algorithms and techniques have been offered in the literature to operate at the maximum power point position because of the non-linearity of the solar power response during weather fluctuations, as shown in [5], [6], and [7]. These methods range from basic ones like voltage and current feedback based MPPT to more sophisticated ones like power feedback based MPPT like the perturbation and observation (P&O) method or the incremental conductance method. Intelligent controls utilizing the MPPT approach were recently shown in [8]. An efficient MPPT-based photovoltaic system ensures quick response times when the climate changes. However, the output obtained from this solar PV array is very low, necessitating extra boosting for many practical applications [5]. To accomplish this boosting, a DC-DC boost converter or a step-up transformer is required [9]. To overcome these drawbacks, a ZSC configuration can be used as a novel power conversion concept [1], [10]. This circuit configuration has many good features with very interesting properties such as improve the power load factor, the cost effective due to a lower component number, reduce the harmonic current and it provides a ride-through during voltage sags [11].

On the other hand, multiphase (with more than three-phase) machine are found to possess several potential benefits over traditional three-phase counterpart [12]. Major benefits are: reduced harmonic voltages, higher reliability and increased power in the same frame [13], [14]. Therefore, multiphase motor drives are extensively used in many applications, not limited to ship propulsion system and vehicle, rolling mills, industries (textile, steel etc.), power plants [15], [16]. In addition, one of the benefits of multi-phase motor drives is possible to combine several series/parallel motors. Such series-connected/parallel-connected two-motor is called drive system [17], [18]. The motors may be controlled individually and operated at various speeds without interfering each other [18], which are of particular importance in industrial applications that requires coordinated operation of two motor drives. On the other side, multilevel power inverters have better performance compared to traditional inverter topologies [9] due their high-power capability, particularly under photovoltaic application. In this context, it has been shown that the combination of these two concepts can lead to additional benefits, as the proposed topology relies on opening the second motor's stator winding neutral point being opened and dual five-phase two-level inverter supplying both winding ends, which is known as ''open-end winding'' (OEW) [15].

This paper presents the combination of the multi machine concept under open-end winding and the ZSC with PV array system to produce an adjustable speed drive. The basic block schematic of the considered configuration is shown in Fig. 1, which comprises of dual-inverter system whose outputs are coupled to ten terminals of SC5PIM-OEW drive. The inverters are connected via ZSC and operated using the SAZE-SVPWM algorithm based on FOC, which controls the SC5PIM-OEW drive input voltages.

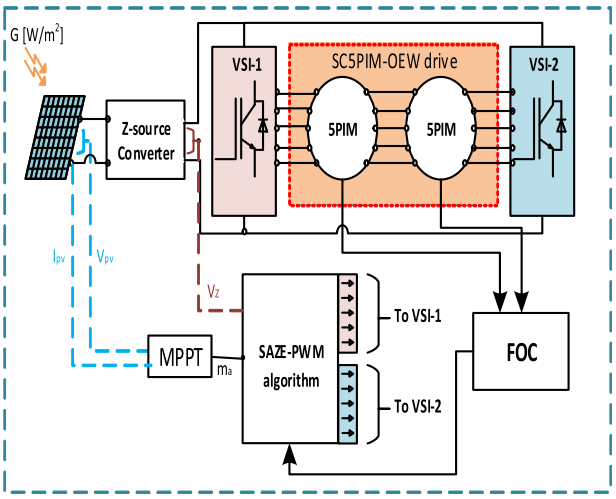

FIGURE 1. The block diagram of studied control system.

The main contributions of this work can be summarized as:

- The novelty of the proposal here discussed is the coupling of the studied SC5PIM-OEW drive with a Z-source and dual-inverter.
- In applications that requires coordinated operation of two motors in either speed/torque control modes, using this proposed topology will result in reduced size and increased efficiency of the overall system.
- SVPWM based-SAZE offers fixed switching frequency and lower harmonics distortion. Therefore, it provides reduced ripples and lower switching losses compared to the works presented in [10], [11], [13], [14], and [15].
- The design and development of FOC algorithm as a speed–flux controller for SC5PIM-OEW drive to track a desired reference, where the main aim is to minimize the tracking error in comparison with the previous works [9], [14], [15].

- The validation of the proposed control strategies of the studied SC5PIM-OEW drive are achieved using real time implementation at various operating points such as variable load torque, high/low speed operation, motor parameter changes, and speed reverse operation.

II. DESCRIPTION OF SC5PIM-OEW DRIVE

The two five-phase stator windings are connected in series in the investigated configuration, as shown in Fig. 2. The two-motors are connected via dual power converter, which are five-phase voltage source inverters (VSI-1 and VSI-2).

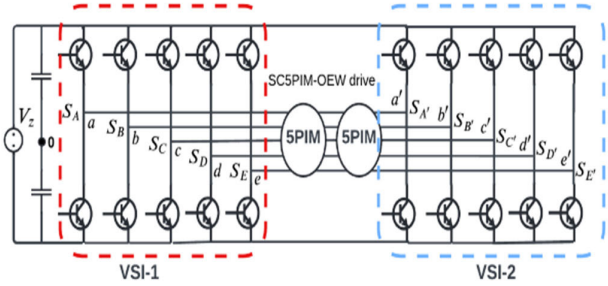

FIGURE 2. The stator windings of two induction motors connected via dual inverter.

A. DUAL-INVERTER SYSTEM

Switching states are employed to model the dual-inverter in the investigated topology [15], the switching function S_M (M can be A, B, C, D, E, A', B', C', D',E') requires the logic generated from the proposed SAZE control. The principal circuit of two inverters presented in Fig. 2 composes of ten poles (a, b, c, d, e and a', b', c', d',e') and twenty switches. On the other side, the pole voltages in a particular phase can be $\pm V_z/2$ based on the switch is turned ON. Thus, the pole voltages at the output of VSI-1 and VSI-2 can be given as:

$$\begin{cases} v_{ao} = \dfrac{S_A V_z}{4}; v_{bo} = \dfrac{S_B V_z}{4}; v_{co} = \dfrac{S_C V_z}{4}; \\ v_{do} = \dfrac{S_D V_z}{4}; v_{eo} = \dfrac{S_E V_z}{4} \end{cases} \tag{1}$$

$$\begin{cases} v_{a'o} = \dfrac{S_{A'} V_z}{4}; v_{b'o} = \dfrac{S_{B'} V_z}{4}; v_{c'o} = \dfrac{S_{C'} V_z}{4}; \\ v_{d'o} = \dfrac{S_{D'} V_z}{4}; v_{e'o} = \dfrac{S_{E'} V_z}{4} \end{cases} \tag{2}$$

The currents flowing in the dual-inverter system are expressed as follows:

$$\begin{cases} i_s = i_Z - i_C \\ i_s = i_{VSI-1} + i_{VSI-2} \end{cases} \tag{3}$$

$$i_s = \frac{i_{aa'}(S_A - S_{A'})}{4} + \frac{i_{bb'}(S_B - S_{B'})}{4} + \frac{i_{cc'}(S_C - S_{C'})}{4} + \frac{i_{dd'}(S_D - S_{D'})}{4} + \frac{i_{ee'}(S_E - S_{E'})}{4} \tag{4}$$

where $i_{aa'}, i_{bb'}, i_{cc'}, i_{dd'}, i_{ee'}$ are stator currents of the SC5PIM-OEW drive and V_z is the output voltage of Z-source converter.

B. TWO-MOTOR DRIVE SYSTEM

The stator windings of two motors are configured as an open-end stator winding and the rotor windings are taken as three-phase. Fig. 3 demonstrates that the SC5PIM-OEW phase transposition rules. It is possible to create a connection table using [17], as illustrated in Table 1.

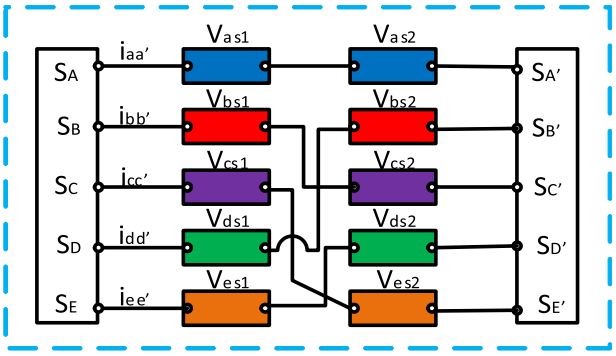

FIGURE 3. The stator windings with open end winding.

TABLE 1. Connectivity matrix for the 5PIM drive.

Phase M1	A	B	C	D	E
First motor	1	2	3	4	5
Phase M2	**A'**	**B'**	**C'**	**D'**	**E'**
Second motor	1	3	5	2	4

According to the connection diagram of SC5PIM drive, it is possible to reconstruct the phase voltages of two five-phase stator windings as [17]:

$$\begin{cases} V_{aa'} = V_{as1} + V_{as2} \\ V_{bb'} = V_{bs1} + V_{bs2} \\ V_{cc'} = V_{cs1} + V_{cs2} \\ V_{dd'} = V_{ds1} + V_{ds2} \\ V_{ee'} = V_{es1} + V_{es2} \end{cases} \tag{5}$$

where $V_{as1}, V_{bs1}, V_{cs1}, V_{ds1}, V_{es1}$ are the stator voltages of first machine, $V_{as2}, V_{bs2}, V_{cs2}, V_{ds2}, V_{es2}$ are the stator voltages of second machine.

The idea of reference frame is used to simplify the differential equations (which are non-linear) by adding a constant inductance term. Park's transformation in synchronous reference frame is used to formulate the motor equations as follows:

$$\begin{bmatrix} V_{ds} \\ V_{qs} \\ V_{xs} \\ V_{ys} \end{bmatrix} = C. \begin{bmatrix} V_{aa'} \\ V_{bb'} \\ V_{cc'} \\ V_{dd'} \\ V_{ee'} \end{bmatrix} = C. \begin{bmatrix} V_{as1} + V_{as2} \\ V_{bs1} + V_{bs2} \\ V_{cs1} + V_{cs2} \\ V_{ds1} + V_{ds2} \\ V_{es1} + V_{es2} \end{bmatrix} \tag{6}$$

Using the Park's transformation, the resulting stator voltage equations for the SC5PIM drive can be expressed as follows:

$$\begin{cases} V_{ds} = R_{s1} i_{ds1} + p\varphi_{ds1} + R_{s2} i_{ds2} + p\varphi_{ds2} \\ V_{qs} = R_{s1} i_{qs1} + p\varphi_{qs1} + R_{s2} i_{qs2} + p\varphi_{qs2} \end{cases} \tag{7}$$

$$\begin{cases} V_{xs} = R_{s1} i_{xs1} + p\varphi_{xs1} + R_{s2} i_{xs2} + p\varphi_{xs2} \\ V_{ys} = R_{s1} i_{ys1} + p\varphi_{ys1} + R_{s2} i_{ys2} + p\varphi_{ys2} \end{cases} \quad (8)$$

Similarly, the rotor voltage equations for the SC5PIM drive are given by:

$$\begin{cases} V_{dr1} = R_{r1} i_{dr1} + \omega_1 \varphi_{qr1} + p\varphi_{dr1} \\ V_{qr1} = R_{r1} i_{qr1} - \omega_1 \varphi_{dr1} + p\varphi_{qr1} \end{cases} \quad (9)$$

$$\begin{cases} V_{dr2} = R_{r2} i_{dr2} + \omega_2 \varphi_{qr2} + p\varphi_{dr2} \\ V_{qr2} = R_{r2} i_{qr2} - \omega_2 \varphi_{dr2} + p\varphi_{qr2} \end{cases} \quad (10)$$

Table 2 summarizes the SC5PIM parameters. Finally, the electromagnetic torque for the studied topology is given:

$$\begin{cases} T_{em1} = 2.5 P_1 M_1 \left(i_{dr1} i_{qs} - i_{qr1} i_{ds} \right) \\ T_{em2} = 2.5 P_2 M_2 \left(i_{dr2} i_{ys} - i_{qr2} i_{xs} \right) \end{cases} \quad (11)$$

where: M_1 and M_2 are the mutual inductances between stator and rotor of SC5PIM drive respectively.

TABLE 2. The SC5PIM parameters.

Designation	First Motor M1	Second Motor M2
Voltage phase	220 V	230 V
Frequency	50 Hz	60 Hz
Stator resistance	10 Ω	10 Ω
Rotor resistance	6.3 Ω	6.3 Ω
Stator/rotor inductance	0.274 H	0.274 H
Mutual inductance	0.258	0.258 H
Moment of inertia	$3*10^{-3}$	$3*10^{-3}$
Friction coefficient	0.166	0.166

III. PV ARRAY POWERED Z-SOURCE CONVERTER

The circuit schematic of PV array with Z-source configuration is presented in Fig. 4. The Z-source converter is triggered by the extracted power from the PV source, which is based on the solar temperature and radiation conditions.

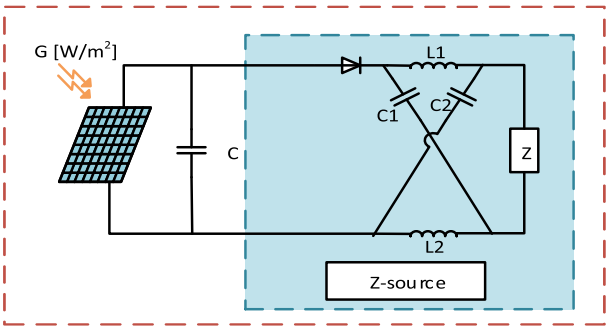

FIGURE 4. The circuit schematic of PV array with Z-source converter.

A. PV ARRAY DESIGN

The electrical circuit for the presented PV array is shown in Fig. 5. A standard 30 − W PV module BLD30 − 36M made

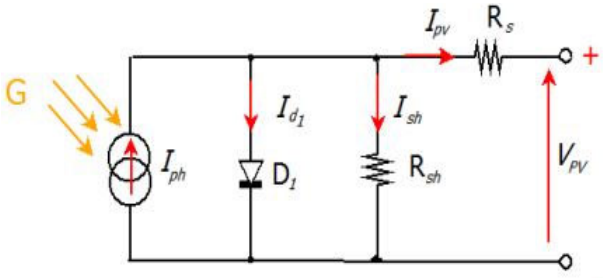

FIGURE 5. The electrical circuit for the PV array.

TABLE 3. Parameters of PV array and Z-source converter.

Designation	Specification
Specification of BLD30-36M Module	
Number of cells per module	36
Maximum power	30 W
Open-circuit voltage	22 V
Short-circuit current	2.21 A
For PV Array	
MPP Voltage	475 V
MPP Power	8.9 kW
MPP Current	Pmpp/Vmp=18.74 A
Module in series	Vmpp/Vmp=27
Module in parallel	Impp/Imp=11
Design Specifications of Z-Source	
Capacitors	4 mF
Split inductor	1mH

by BLD Solar is taken into consideration for the design of the PV array [19]. Since power rating of studied topology is 8.5 kW, a PV array of 8.9 kW is designed. Table 3 summarizes the electrical specifications of a chosen PV module. Thus, the mathematical model describing the performance of PV array output under solar temperature and radiation conditions is given by [6]:

$$I_{pv} = I_{ph} - I_d - I_{sh} \quad (12)$$

$$I_d = I_0 \left[e^{\left(\frac{V_{pv} + R_s I_{pv}}{A.N_s.V_t} \right)} - 1 \right] \quad (13)$$

$$I_{sh} = \left(\frac{V_{pv} + R_s I_{pv}}{R_{sh}} \right) \quad (14)$$

$$I_{pv} = I_{ph} - I_o \left[e^{\left(\frac{V_{pv} + R_s I_{pv}}{A.N_s.V_t} \right)} - 1 \right] - \left(\frac{V_{pv} + R_s I_{pv}}{R_{sh}} \right) \quad (15)$$

$$V_t = \frac{k.V_{pv}}{q} \quad (16)$$

where: V_{pv} is the PV cell voltage, I_{pv} is the generated PV current, I_{ph} is the photocurrent, I_o is the diode saturation current, k is the Boltzmann constant, R_s and R_{sh} are the PV cell series/ parallel resistances, N_s is the number of cells connected in series, A is the diode ideality factor, q is the electron charge, V_t corresponds to the thermal voltage.

B. Z-SOURCE CONFIGURATION

A Z-source configuration was proposed by [1] to overcome the existing problems in the conventional topologies. In this configuration, the interface between the input of a dual-inverter structure and the output of a PV array is a symmetrical impedance network., this circuit network contains two split inductor L_1, L_2 and two capacitors C_1, C_2 connected in X shape [10], [11], as illustrated in Fig. 6. In the shoot-through zero state of this topology, both the upper and lower switches are turned on simultaneously. This state cannot be given by a standard voltage source because harm could result from activating switches on the same leg.

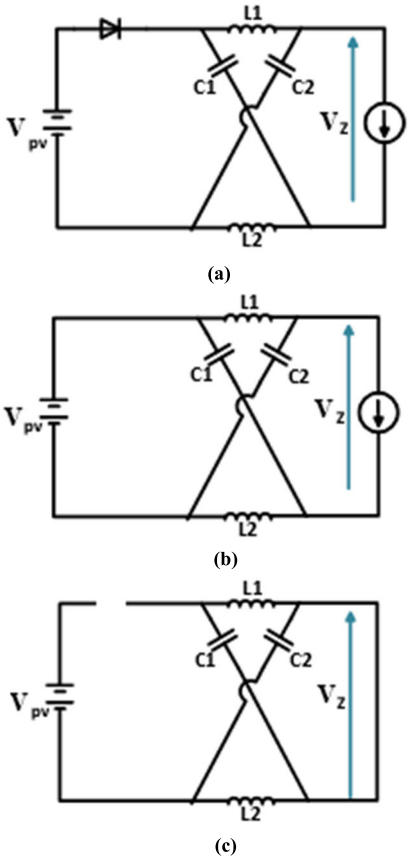

FIGURE 6. The Z-Source circuit configuration (b) non-shoot through mode (c) shoot through mode.

The DC output voltage to the Z-source network is expressed as follows:

$$V_z = \frac{V_{pv}}{1-2D} = H.V_{pv} \tag{17}$$

where, D is the shoot through duty ratio, V_{pv} is the DC input voltage and H is the boost factor.

IV. DSAZE-SVPWM AND MPPT ALGORITHM

As described in Fig. 1, the MPPT component of the algorithm incorporates motor drive to draw the highest amount of power possible from the PV source, ensuring effective PV array utilization. Further, rotor flux-oriented control is incorporated into the sample-averaged zero-sequence elimination (SAZE) method based on space vector pulse width modulation (SVPWM) component. It keeps the motor's rated flux constant, preserving the machine's maximum torque capacity. Thus, maintaining the maximal torque also contributes to the best possible use of the input source. Fig. 7 presents the flow chart of the MPPT and DSAZE-SVPWM strategy used in the proposed control for the studied SC5PIM-OEW drive.

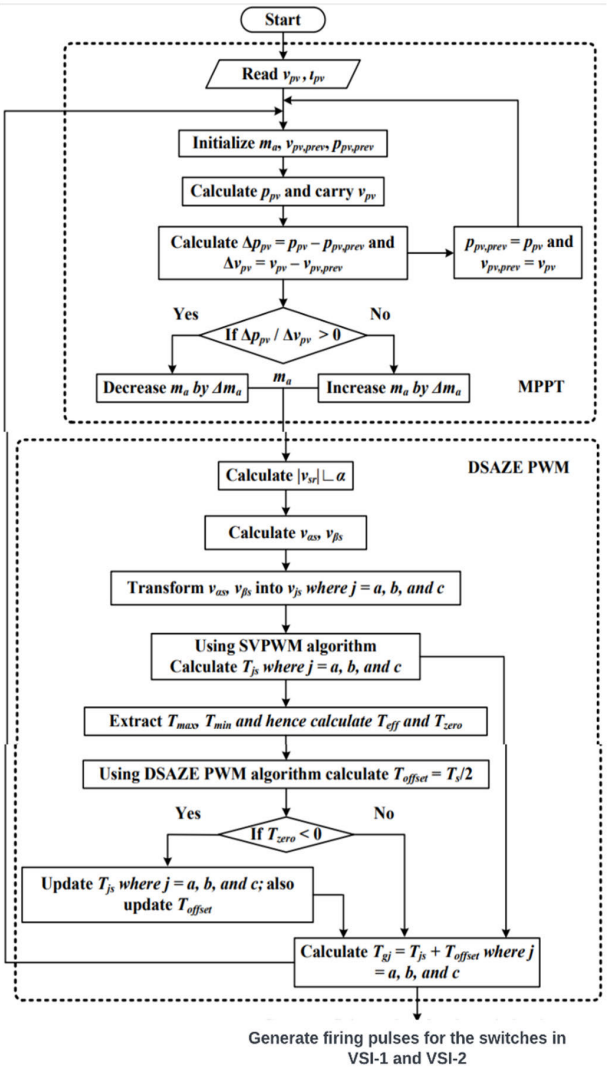

FIGURE 7. Flow chart of the MPPT and DSAZE-SVPWM strategy used in the proposed control.

A. MPPT ALGORITHM

Due to the non-linearity of the solar PV response, the output current and voltage depend on the fluctuation in the weather conditions [7], a number of MPPT techniques are proposed by various researchers to extract optimum power during the variation of the climate status [7], [8].

The MPPT algorithm helps in the effective tracking of maximum power from the PV source. The algorithm first

senses the generated PV current (I_{pv}) and the PV cell voltage (V_{pv}) for determining the power (P_{pv}). The slope of the operating point is calculated by comparing the calculated power and sensed voltage values to their prior value. The correction for modulation index (m_a) is then determined by the considered slope. According to the flowchart in Fig. 7, the value of m_a is changed (incremented or decremented) until the operating point is close to MPP. The computed value of m_a is utilized by the DSAZE-SVPWM strategy.

B. DSAZE-SVPWM STRATEGY

The instantaneous five-phase reference voltage for VSI-1 are derived from the magnitude of the reference voltage vector created by the MPPT output and FOC strategy. The switching method [20] is then used to determine the gating time Tgj (j=a, b, c, d, e) for the top switches of VSI-1. For the purpose of computing the effective time (time for which all the active vectors are switched), this method requires instantaneous values of the reference phase voltage [20]. It is possible to move the position of effective time period so that the offset time is equal to Ts/2 during a switching period. The DSAZE-SVPWM approach takes advantage of this property to get rid of the zero-sequence voltage. The gating time Tgj' (j=a', b', c', d', e') for the top switches of VSI-2 are readily determined using the gating time for VSI-1, using the fact that both the reference voltage vectors for VSI-1 and VSI-2 are in the phase opposition as follows:

$$T_{gj'} = T_s - T_{gj} \tag{18}$$

V. REAL-TIME RESULTS AND DISCUSSION

To study and verify the dynamic behavior of the proposed system for operation with single-stage PV array, real-time simulations were conducted using OPAL-RT 4500. The solar PV array, SC5PIM-OEW drive, Z-source converter and dual-inverter system are modeled on OPAL-RT simulator (OP 4500), as shown in Fig.8.

The reference values of the irradiance and temperature at two different levels of irradiance (600 W/m2, and 1000 W/m^2) with fixed ambient temperature of 25 °C, are shown in Fig. 9. The Fig.10 to Fig. 12 show the generated voltage and current of PV array and Z-source converter respectively. It can be observed that the generated voltage and current of solar PV array with MPPT-SAZE technique offers a sudden increase in voltage during irradiance change. The waveform of applied voltage to 5-phase induction motor 1 is presented in Fig. 13.

A. HIGH SPEED VARIATION

To show the feasibility of the designed control algorithms, the first conducted test was carried out under high speed and load torque variation. It can be seen from the results shown in Fig. 14 that real speed for each motor (motor-1 and motor-2) follows the respective reference speed with an acceptable response time compared to the work presented in [9], [14], [15], [21], [22], and [23], where it can be observed that the speed error is around zero during steady state, as shown in Fig. 15. This confirms the effectiveness of the proposed techniques. Furthermore, the developed torque

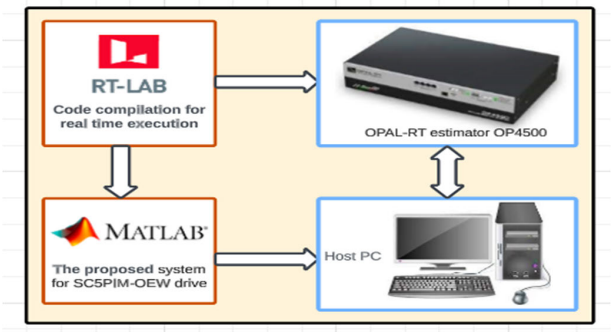

(a)

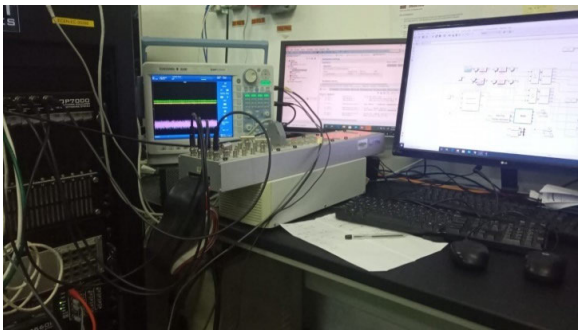

(b)

FIGURE 8. The real-time platform of proposed system based on OPAL-RT simulator: (a) connection diagram, (b) realistic setup.

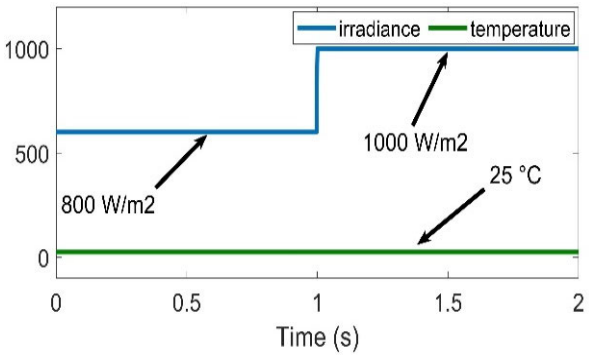

FIGURE 9. The reference values of the irradiance and temperature.

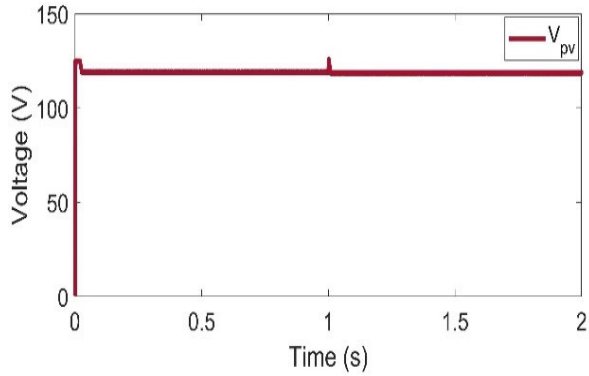

FIGURE 10. The generated voltage of solar PV array.

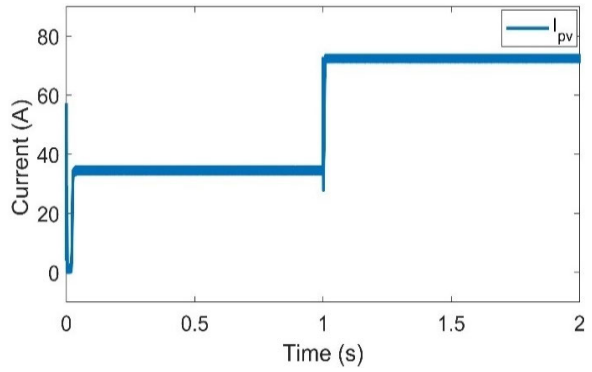

FIGURE 11. The generated current of solar PV array.

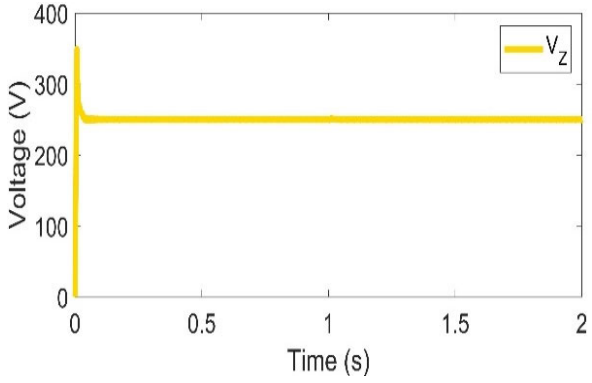

FIGURE 12. The generated voltage of Z-source converter.

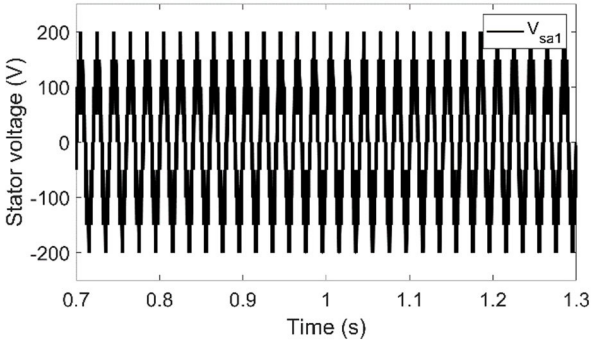

FIGURE 13. The waveform of applied voltage to 5-phase induction motor 1.

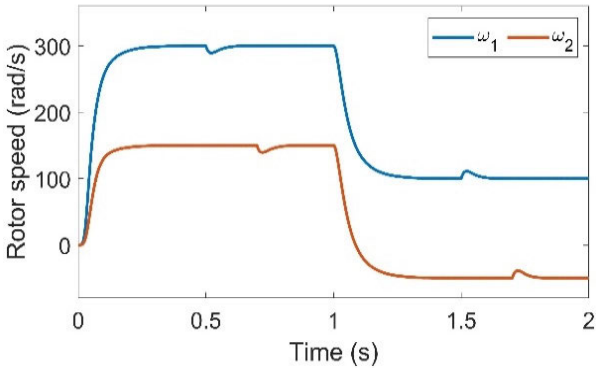

FIGURE 14. Response of speeds.

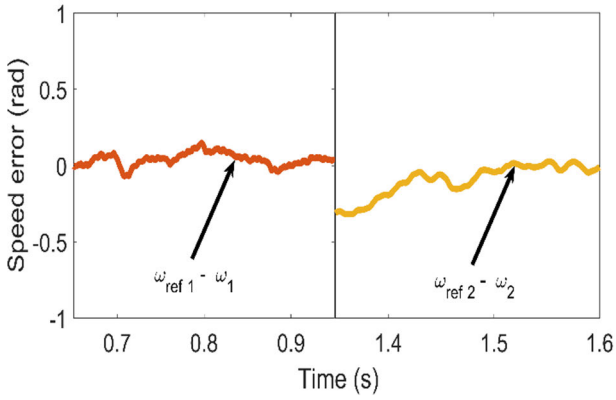

FIGURE 15. Speed tracking errors.

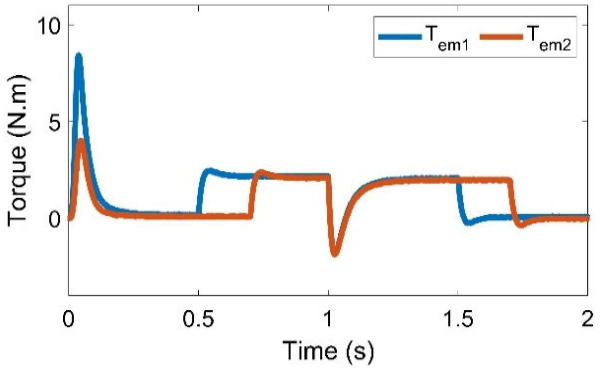

FIGURE 16. Response of developed torque.

perfectly follows its reference as shown in Fig.16, which is reached quickly with low torque ripples compared to the results presented in many earlier works such as in [10], [13], [14], and [15]. Thus, a diminution in developed torque ripple helps in reducing the currents ripple and which in turn improves the SC5PIM-OEW performance. As can be seen from Fig. 17 and Fig.18 the values of stator currents of each motor increase with respect to the torque requirements with different amplitude and frequency. Hence, an increase or decrease in the reference speed will result in the corresponding increase in current values of SC5PIM-OEW drive. Last subplot of Fig. 19 presents the response of the two components of the rotor flux. It can be seen that decoupled control is maintained using FOC-SVPWM strategy. Furthermore, in contrast to the works reported in [10] and [14], the load torque variation has no effect on performance.

B. LOW SPEED OPERATION

In this test, the SC5PIM-OEW topology is tested at a low speed with parameters variation. In order to study the effect of the resistances variation on the performance of the studied topology, the motors are started with its initial stator resistance value $R_{s1} = R_{s2} = 10\Omega$, after 0.8s and 1s, respectively

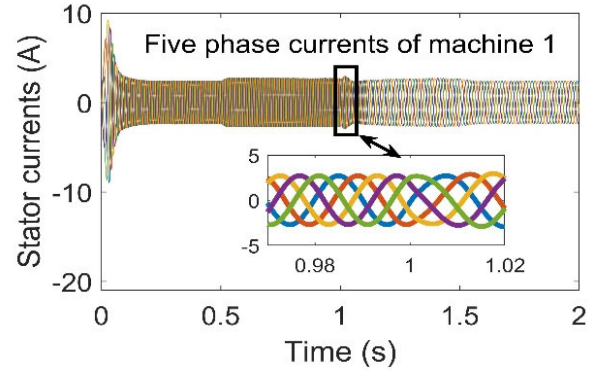

FIGURE 17. The values of stator currents of motor 1.

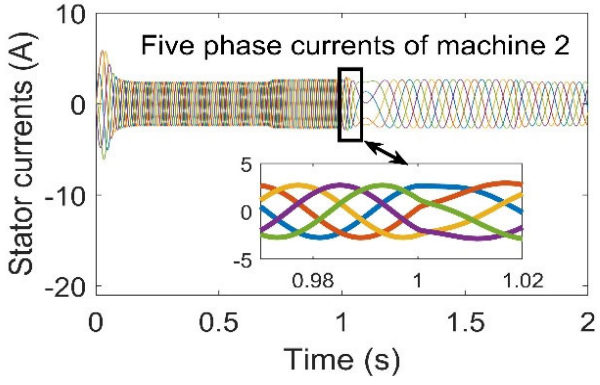

FIGURE 18. The values of stator currents of motor 2.

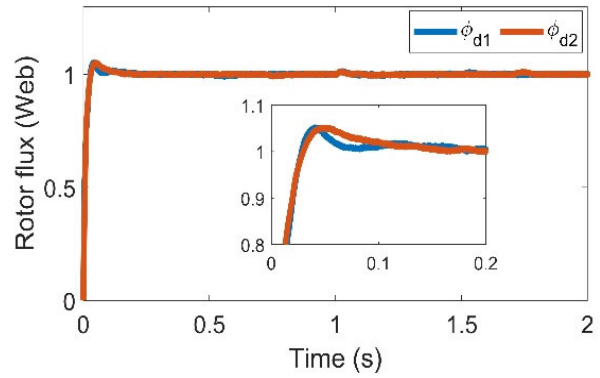

FIGURE 19. Response of rotor flux.

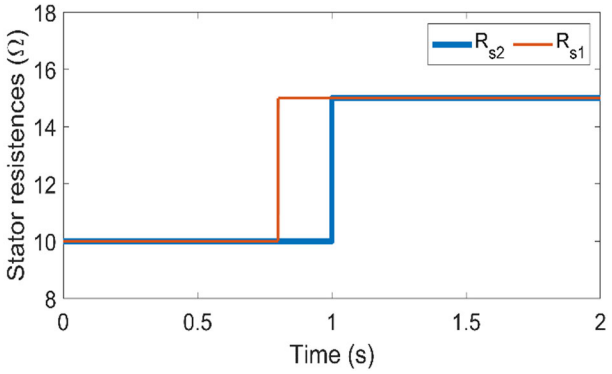

FIGURE 20. Response of stator resistances.

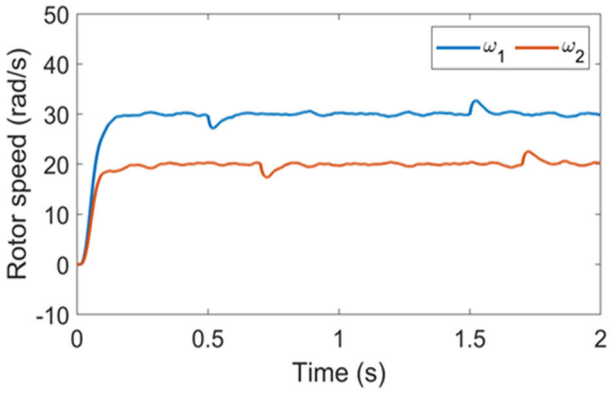

FIGURE 21. Response of *speeds*.

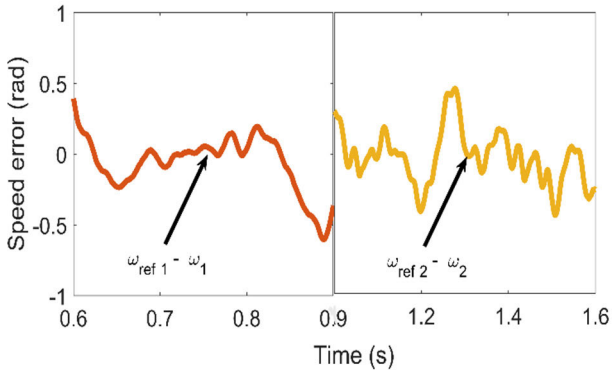

FIGURE 22. Speed tracking errors.

R_{s1} and R_{s2} are changed to $R_{s1} = R_{s2} = 15\Omega$, as shown in Fig.20. As can be seen from Fig. 21 the system exhibits good ability to maintain the real speed (Motor1 or Motor2) close to the reference one during low-speed operation. Furthermore, results indicate that due to the precise control of motor speed, the SC5PIM-OEW drive does not lose stability during operation at low speed. This proves the robustness and effectiveness of the proposed control law under parameter variations, which can change from the nominal ones according to motor temperature and operating condition. The reference speed is compared with the measured one as presented in Fig. 22. Clearly, the maximum speed error is found to be less than 0.5 rad/s in the steady-state. As can be seen in Fig. 23, the developed torque presents high dynamic with fast response and it is equal to the load torque in steady state. The five phase stator currents of the studied SC5PIM-OEW drive are shown in Fig. 24 and Fig. 25. It is clear that the currents behave according to the dynamic behavior of the motor. Fig. 26 illustrates the rotor flux. It can be observed that even if the motor resistance changes, the proposed method still gives a good estimate of rotor flux.

Response of SC5PIM-OEW drive under proposed control are summarized in Table 4.

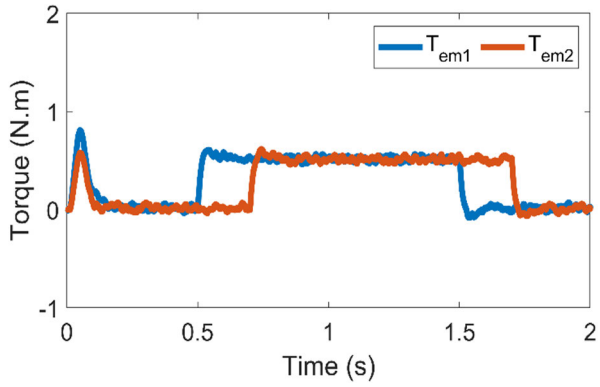

FIGURE 23. Response of developed torque.

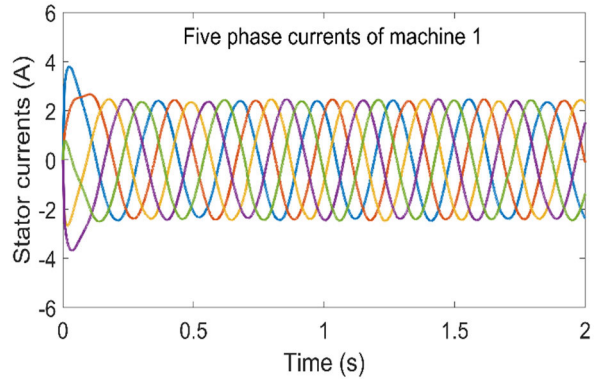

FIGURE 24. The values of stator currents of motor 1.

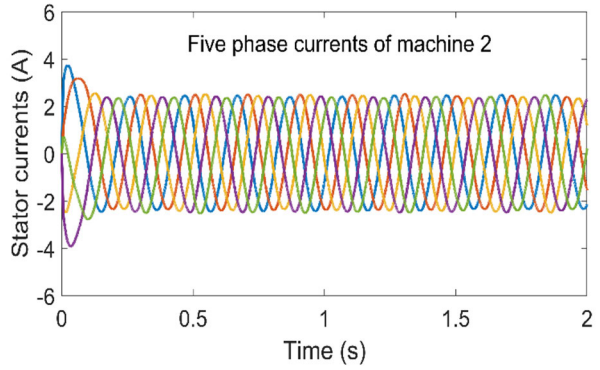

FIGURE 25. The values of stator currents of motor 2.

VI. CONCLUSION

This paper introduces a single-stage solution for solar PV array powered series-connected 5-phase induction motors under OEW supplied off a Z-source and dual-inverter. The studied motor topology is operated using decoupled MPPT technique along with SAZE-SVPWM algorithm based on rotor flux-oriented control in order to extract optimum power from the PV modules and efficient use the two-motor.

The superiority and efficacy of the suggested control approaches are investigated in real time simulation by using OPAL-RT 4500 simulator. It is possible to conclude from the results that were obtained that the suggested method offers a good way to regulate the multi-phase induction machine with excellent performance. The suggested method can be used with inexpensive microcontrollers and is not hindered by computing complexity. Such advantages make it a promising candidate for industrial applications.

TABLE 4. Response of SC5PIM-OEW drive.

Speed	Rise time	Setting time	Maximum speed error
High speed	0.18 s	0.2 s	0.14 rad/s
Low speed	0.16 s	0.2 s	0.5 rad/s

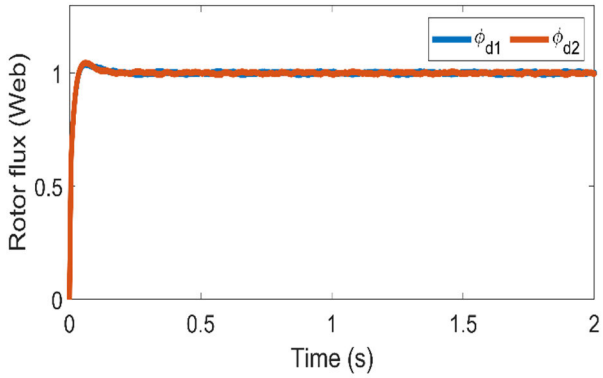

FIGURE 26. Response of rotor flux.

REFERENCES

[1] K. D. Dipak, K. S. Pradip, and S. Bidyadhar, "Spider monkey optimization (SMO)—Lattice Levenberg–Marquardt recursive least squares-based grid synchronization control scheme for a three-phase PV system," *Arch. Electr. Eng.*, vol. 31, no. 3, pp. 707–730, 2021.
[2] N. Ramachandran, S. Murugan, C. Vinayagam, and P. K. Balachandran, "Real-time implementation of a seven-level multilevel DC link inverter for solar PV system during partial shading," *Electr. Power Compon. Syst.*, vol. 51, no. 18, pp. 2125–2134, Nov. 2023.
[3] S. Lalouni, D. Rekioua, T. Rekioua, and E. Matagne, "Fuzzy logic control of stand-alone photovoltaic system with battery storage," *J. Power Sources*, vol. 193, no. 2, pp. 899–907, Sep. 2009.
[4] T. Khatib, I. A. Ibrahim, and A. Mohamed, "A review on sizing methodologies of photovoltaic array and storage battery in a standalone photovoltaic system," *Energy Convers. Manage.*, vol. 120, pp. 430–448, Jul. 2016.
[5] A. Talha, H. Boumaaraf, and O. Bouhali, "Evaluation of maximum power point tracking methods for photovoltaic systems," *Arch. Control Sci.*, vol. 21, no. 2, pp. 151–165, Jan. 2011.
[6] M. Menzou, S. Khadar, and M. E. Kobbi, "RT-lab based real-time simulation of a new solar PV array powered open-end winding induction motor using a boost DC–DC converter," in *Proc. 1st Int. Conf. Renew. Solutions Ecosystems: Towards Sustain. Energy Transition (ICRSEtoSET)*, May 2023, pp. 1–5.
[7] H. A. Attia and B. N. Getu, "Design & simulation of a solar tracking system for optimum energy absorption," *Int. J. Thermal Environ. Eng.*, vol. 8, no. 1, pp. 17–24, 2014.
[8] H. Attia, "Fuzzy logic controller effectiveness evaluation through comparative memberships for photovoltaic maximum power point tracking function," *Int. J. Power Electron. Drive Syst. (IJPEDS)*, vol. 9, no. 3, p. 1147, Sep. 2018.
[9] B. N. Reddy, B. S. Goud, C. N. Sai Kalyan, P. K. Balachandran, B. Aljafari, and K. Sangeetha, "The design of 2S2L-based buck-boost converter with a wide conversion range," *Int. Trans. Electr. Energy Syst.*, vol. 2023, pp. 1–17, Apr. 2023.
[10] T. Minan, Y. Shangmei, Z. Kaiyue, W. Qianqian, L. Chenggang, and D. Xuewang, "Model predictive direct power control of energy storage quasi-Z-source grid-connected inverter," *Arch. Electr. Eng.*, vol. 71, no. 1, pp. 21–35, 2022.

[11] B. H. Haithem, K. Laroussi, and S. Khadar, "Sliding mode control of five phase PMSM fed by Z-source inverter: Application to renewable energy," in *Proc. 1st Int. Conf. Renew. Solutions Ecosystems*, May 2023, pp. 1–5.
[12] S. Khadar, A. Y. Abdelaziz, Z. M. S. Elbarbary, and M. A. Mossa, "An improved sensorless nonlinear control based on SC-MRAS estimator of open-end winding five-phase induction motor fed by dual NPC inverter: Hardware-in-the-loop implementation," *Machines*, vol. 11, no. 4, p. 469, Apr. 2023.
[13] S. Khadar and H. Benguesmia, "Load torque estimation in sensorless speed control of dual star induction machine using only voltage and current measurements," in *Proc. 5th IEEE Int. Conf. Mech. Energy*, 2019, pp. 1–6.
[14] S. Khadar, "Influence of a different fault scenarios on the properties of multi-phase induction machine," *Algerian J. Eng. Technol.*, vol. 2, pp. 11–21, Aug. 2020.
[15] K. Saad, K. Abdellah, H. Ahmed, and A. Iqbal, "Investigation on SVM-backstepping sensorless control of five-phase open-end winding induction motor based on model reference adaptive system and parameter estimation," *Eng. Sci. Technol., Int. J.*, vol. 22, no. 4, pp. 1013–1026, Aug. 2019.
[16] A. S. Abdel-Khalik, M. S. Abdel-Majeed, and S. Ahmed, "Effect of winding configuration on six-phase induction machine parameters and performance," *IEEE Access*, vol. 8, pp. 223009–223020, 2020.
[17] A. Iqbal, S. Vukosavic, E. Levi, M. Jones, and H. A. Toliyat, "Dynamics of a series-connected two-motor five-phase drive system with a single-inverter supply," in *Proc. Fourtieth IAS Annu. Meeting. Conf. Rec. Ind. Appl. Conf.*, 2005, pp. 12–18.
[18] M. Jones, E. Levi, and S. N. Vukosavic, "Independent control of two five-phase induction machines connected in parallel to a single inverter supply," in *Proc. 32nd Annu. Conf. IEEE Ind. Electron.*, Nov. 2006, pp. 1257–1262.
[19] *BLD30-36M Standard Solar PV Module Specifications*. Accessed: Jun. 12, 2015. [Online]. Available: http://www.alliancesolar.com.au/images/Boucher/
[20] S. Khadar, T. B. Ali, H. Benguesmia, M. Fadhila, A. Kouzou, and M. M. Rezaoui, "Improved performance of backstepping control of an open-end stator winding five-phase induction motor with the fundamental and harmonic currents," in *Proc. Int. Conf. Adv. Electr. Eng. (ICAEE)*, Nov. 2019, pp. 1–6.
[21] A. Hosseyni, R. Trabelsi, M. F. Mimouni, A. Iqbal, and R. Alammari, "Sensorless sliding mode observer for a five-phase permanent magnet synchronous motor drive," *ISA Trans.*, vol. 58, pp. 462–473, Sep. 2015.
[22] A. Kirad, S. Groini, and Y. Soufi, "Improved sensorless backstepping controller using extended Kalman filter of a permanent magnet synchronous machine," *Bull. Electr. Eng. Informat.*, vol. 11, no. 2, pp. 658–671, Apr. 2022.
[23] K. Saad, K. Abdellah, and T. B. Ali, "Advanced fault-tolerant control of multiphase induction motor drives in EV," in *Proc. 1st Int. Conf. Sustain. Renew. Energy Syst. Appl. (ICSRESA)*, Dec. 2019, pp. 1–5.

SAAD KHADAR received the bachelor's and master's (Hons.) degrees from the University of Msila, Algeria, and the Ph.D. degree in electrical engineering from the University of Djelfa, in 2021. He joined as a Graduate Assistant with the Smart Grid Center, Texas A&M University at Qatar, Doha, in 2020. He has research experience at many universities in many countries, including Qatar, Poland, Turkey, and Algeria. He is currently a Professor with the Ziane Achour University of Djelfa. He has supervised many research projects on multiphase machine control, power electronics converters, and renewable energy systems. He has published more than 53 journal articles and conference papers. His research interests include electric drives, power electronic converters, renewable energy, diagnostics, and fault-tolerant control. He is a reviewer of several journals and conferences.

ALMOATAZ Y. ABDELAZIZ (Senior Member, IEEE) received the joint Ph.D. degree in electrical engineering according to the channel systems from Ain Shams University and Brunel University, U.K., in 1996. He has been a Professor of electrical power engineering with Ain Shams University, since 2007. He is currently delegated with the Faculty of Engineering and Technology, Future University in Egypt, which he was the Vice Dean of Education and Students Affairs, from 2018 to 2019. He has authored or co-authored more than 550 refereed journals and conference papers, 50 book chapters, and eight edited books with Elsevier, Springer, and CRC Press. In addition, he has supervised more than 80 master's and 40 Ph.D. theses. His research interests include the applications of artificial intelligence and evolutionary and heuristic optimization techniques to power system planning, operation, and control. He is a member of Egyptian Sub-Committees of IEC, CIGRE, and CIRED. He has been awarded many prizes for distinct research and international publishing from Ain Shams University and Future University in Egypt. He received the Ain Shams University Appreciation Award in Advanced Technological Engineering Sciences, in 2022. He is the Chair of the IEEE Education Society Chapter in Egypt. He is an Editor of *Electric Power Components and Systems* (T&f) and *Energy and AI* (Elsevier) journals. He is an editorial board member, an editor, an associate editor, and an editorial advisory board member of many international journals.

Z. M. S. ELBARBARY was born in Kafrelsheikh, Egypt, in 1971. He received the B.Sc., M.Sc., and Ph.D. degrees in electrical engineering from Menoufia University, Egypt, in 1994, 2002, and 2007, respectively. In 2009, he joined Kafrelsheikh University as an Assistant Professor, where he became a Full Professor of power electronics, in June 2022. In 2016, he was a Research Visitor with Ghent University, Ghent, Belgium, for two months. His research interests include control of electrical machines, senseless control, applications of power electronics, real-time control using digital signals processing, and renewable energy applications.

MAHMOUD A. MOSSA received the bachelor's and master's degrees in electrical engineering from the Faculty of Engineering, Minia University, Egypt, in 2008 and 2013, respectively, and the Ph.D. degree in electrical engineering, in April 2018. Since January 2010, he has been an Assistant Lecturer with the Electrical Engineering Department (EED), Faculty of Engineering, Minia University. In November 2014, he joined the Electric Drives Laboratory (EDLAB), University of Padova, Italy, for his Ph.D. research activities. Since May 2018, he has been an Assistant Professor with the Electrical Engineering Department, Minia University. He occupied a postdoctoral fellow position with the Department of Industrial Engineering, University of Padova, in 2021 and 2022. He is currently an Associate Professor with the Electrical Engineering Department, Faculty of Engineering, Minia University. He has edited three books and authored two books till now. His research interests include renewable energy systems, power management, optimization, electric machine drives, power electronics, and load frequency control. He served as a guest editor for different international journals. He is an Active Associate Editor of *International Journal of Robotics and Control Systems*.